Deep Resources Engineering 2 (2025) 100186

Contents lists available at ScienceDirect

Deep Resources Engineering

journal homepage: www.keaipublishing.com/en/journals/deepre/

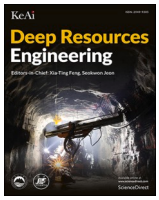

Full Length Article

Analysis of tunnel water inrush accidents induced by stratum collapse models

Jiayao Chen [a], Dingli Zhang [a,*], Mingyue Su [a], Xiaotian Liu [a], Xiangdong Mi [b]

[a] Key Laboratory for Urban Underground Engineering of Ministry of Education and School of Civil Engineering, Beijing Jiaotong University, Beijing 100044, China
[b] Zhuhai Urban Construction Group Co., Ltd, Zhuhai 519000, China

ARTICLE INFO

Keywords:
Rock tunnels
Water inrush
Stratum collapse
Accident analysis

ABSTRACT

As tunnel engineering progresses, the complexity of geological strata and the presence of water bodies beneath tunnels have exacerbated the risk of water inrush incidents. Mutation theory is utilized to elucidate the mechanisms underlying stratum collapse-induced water inrush, with the Shijingshan Tunnel's water inrush pattern identified as stratum collapse-induced. Finite element method (FEM) numerical models were developed for four conditions: original tunnel, Grade III surrounding rock, advanced grouting reinforcement, and sectional excavation. The evolution of the plastic zone, deformation, and support forces in the surrounding rock was compared across these models. The study demonstrates that shear failure of the rock mass, induced by concentrated stress and water pressure during excavation, results in the formation of water inrush pathways. Advanced grouting and sectional excavation effectively reduced the plastic zone and vertical deformation. This mitigation lessened support damage and decreased the likelihood of stratum collapse. This paper offers technical support and case analysis for the prevention of stratum collapse-induced water inrush in underwater blasting operations.

1. Introduction

When tunnel engineering projects pass beneath water bodies, significant geological hazards such as water inrush and mud gushing often occur, posing substantial threats to construction safety and project stability [1]. The risk of water inrush due to stratum collapse is significantly increased, especially in areas with weak fractured zones, karst development, or water-rich formations [2]. In this mode, water inrush typically occurs alongside large-scale instability and collapse of the surrounding strata, often resulting in severe damage to the tunnel excavation face or lining structure [3]. Traditional water inrush prevention technologies and monitoring methods often fail to predict and prevent such disasters in a timely manner. Comprehensive research on water inrush mechanisms and stratum collapse under different geological conditions is essential. Such work enhances the safety and reliability of tunnel construction [4,5].

Existing research primarily focuses on three areas: theoretical studies, laboratory experiments, and numerical simulations. In the realm of theoretical research, Zhang et al. [1] proposed three water inrush modes for subsea tunnels, revealing their mechanisms and clarifying disaster evolution characteristics and methods for characterizing strata deformation. [4]. Shen et al. [6] and Zhang et al. [7] employed limit equilibrium theory to analyse the mechanical mechanisms of water inrush in subsea tunnels and explored the factors influencing critical water pressure. Cacciuttolo, C et al. [8] systematically studied water inrush mechanisms, control techniques, and related issues in underwater tunnels using the complex variable function method [9]. Niu et al. [10] from a fluid dynamics perspective, analyzed hydraulic issues in subsea tunnels and established a flow regime system based on engineering water environment response. [11]. These methods are primarily based on physical and mathematical models, which can systematically describe and predict the behaviour and mechanisms of water inrush [12]. However, they often require the simplification of complex geological conditions and hydrological processes, which may affect the accuracy of predictions by neglecting certain real-world factors. On the other hand, laboratory experiments can provide detailed data under actual conditions, allowing for the analysis of the impact of different hydrological and geological factors on tunnels [13,14]. For instance, Zhang et al. [15] used model tests to study the water inrush mechanism at tunnel base slabs. However, large-scale or complex experiments require substantial equipment investment and experimental costs [16,17].

* Corresponding author.
E-mail addresses: jychen1@bjtu.edu.cn (J. Chen), dlzhang@bjtu.edu.cn (D. Zhang).

https://doi.org/10.1016/j.deepre.2025.100186
Received 13 February 2025; Received in revised form 22 April 2025; Accepted 24 April 2025
Available online 24 April 2025

Numerical simulations can integrate theoretical models and experimental data, taking into account more complex geological and hydrological conditions while performing dynamic analyses. The commonly used finite difference software, finite element method (FEM), has been applied to study the instability mechanisms of surrounding rock masses [18–20]. Zhao et al. [21] simulate the seepage damage behaviour during the water inrush process in rock masses by coupling mechanical equations with seepage continuity equations [22], [23]. Li et al. employed numerical simulation methods to reveal the influence of parameters such as initial support, secondary lining, and grouting reinforcement on tunnel water seepage and external water pressure on the lining [24]. Shekari conducted fluid-solid coupling numerical simulations for subsea tunnels, demonstrating the significant impact of groundwater seepage on the deformation of the surrounding rock mass [25,26]. However, these studies neglect the nonlinear and dynamic evolution characteristics of rock mass mechanical behaviour, making it challenging to predict and control the sudden instability processes of surrounding rock in underwater tunnels [27,28]. Therefore, the theory of catastrophe is introduced to analyse the water inrush mechanism associated with stratum collapse. Catastrophe theory effectively describes the abrupt changes in complex systems under small perturbations, providing theoretical support for predicting the critical instability state of geological hazards. Catastrophe theory, via potential function cusp models, characterizes the system's discontinuous shift from stability to instability. This makes it well-suited for modeling water inrush caused by shear–hydraulic coupling. It can also describe the evolutionary processes of sudden disasters such as seepage failure and layered collapse, aiding in the prediction of critical instability points and enhancing the safety of tunnel construction. And numerical simulations are employed to validate results under various working conditions [29,30].

However, there are still some shortcomings in the research on the water inrush mechanism associated with stratum collapse [27,31]. Existing studies mainly address hydraulic characteristics of inrush points and localized rock mechanical properties. However, the coupled effects during overall stratum instability remain insufficiently understood. [32]. Traditional studies often analyze individual factors in isolation, failing to reveal the coupled mechanisms of multiple influencing factors. For example, the limit equilibrium method neglects the dynamic impact of seepage forces on the evolution of the sliding surface, while pure seepage models do not account for fracture development induced by excavation unloading. This study integrates catastrophe theory with a fluid-solid interaction model to incorporate the synergistic effects of multiple factors, thereby establishing the critical conditions for water inrush. Numerical simulation techniques have shown strong potential in analyzing strata response behavior. However, they face limitations in modeling dynamic collapse and water inrush under complex geological conditions. [33]. A comprehensive theoretical framework for water inrush mechanisms associated with stratum collapse is essential. This should build on existing research and be further validated through numerical simulations and case studies [34,35].

By establishing a systematic stratum collapse-induced water inrush model, this study analyses the causes of accidents when tunnels pass beneath water bodies. The formation mechanism of water inrush induced by stratum collapse is systematically elucidated through theoretical derivations and field investigations. Key influencing factors and operational mechanisms are identified. Based on numerical simulation methods, the constructed water inrush model is applied to specific tunnel engineering scenarios. Through analysing the structural response patterns under different geological conditions and external loads, the dynamic coupling process between strata instability and water inrush is explored [36]. Typical tunnel water inrush accidents are analyzed to summarize their causes and developmental patterns. This provides theoretical guidance and technical support for the design and risk prevention of future projects. The paper is divided into three main sections: first, the mechanism of the stratum collapse-induced water inrush model is analysed; second, the mechanism is incorporated into numerical models to study the structural response patterns of tunnels; and third, based on actual tunnel accidents, the causes of accidents are systematically analysed to provide references for engineering practice.

2. Typical tunnel water inrush modes and their mechanisms

Different water inrush modes may occur depending on the tunnel's geological conditions, groundwater connectivity, and construction disturbances. The formation mechanisms and evolutionary processes of each water inrush mode typically exhibit significant differences [37].

2.1. Typical water inrush modes

Through comprehensive analysis of tunnel water inrush cases, the primary geological causes are identified. These include rock masses with joint fissures, fully weathered weak rocks, and fault fracture zones. Considering the shallow overburden and unlimited water supply in underwater tunnels, water inrush is classified into three modes. These are hydraulic fracturing, stratum collapse, and structural surface sliding. [4].

The first mode is hydraulic fracturing-induced water inrush, commonly occurring in rock masses with developed joint fissures. High hydrostatic pressure causes fissures to extend along existing paths. When the impermeable layer's strength is insufficient, the fissures develop and connect the surface and tunnel excavation face, triggering a water inrush [38,39]. The second mode is stratum collapse-induced water inrush, which occurs when tunnels pass through fully weathered weak rock masses. The collapse of the strata, caused by shear slip zones, reduces the strength and thickness of the impermeable layer, which can no longer withstand the overlying water pressure [40]. This leads to cracking of the tunnel surrounding rock and connectivity with the overlying water body, often accompanied by overall instability of the surrounding rock. The third mode is structural surface slip-induced water inrush, commonly found in fault fracture zones. This occurs when structural interfaces are exposed, which may involve direct excavation into water-bearing surfaces. Differential deformation due to mechanical property variations causes displacement, misalignment, or opening [41].

2.2. Mechanism of stratum collapse-induced water inrush

When tunnels pass through weakly fractured rock masses, stress concentration may lead to localized instability or collapse of the surrounding rock. On one hand, this increases the influence range of the tunnel excavation, resulting in aggravated uneven settlement of the surrounding rock [42]. On the other hand, it damages the structural integrity of the surrounding rock. If not addressed promptly, the collapse range will continue to expand under concentrated stress. If the overlying soil and rock layer thickness is less than the critical thickness, the collapse range will extend to the bedrock, triggering overall stratum collapse and water inrush disasters [43]. Therefore, the critical thickness of the overlying rock layer is an important criterion for determining whether a stratum collapse-induced water inrush accident will occur in underwater tunnels. This section will use catastrophe theory to establish a prediction model for stratum collapse-induced water inrush in underwater tunnels.

2.2.1. Prediction model for stratum collapse-induced water inrush

As indicated by the dashed line in Fig. 1, the strata slip surface caused by tunnel excavation generally takes the form of a parabolic shape. Assuming the strata slip surface to be a straight line (the solid line in Fig. 1), The Shijingshan Tunnel passes through highly weathered granite, where the rock mass is fractured with poor strength homogeneity. The shear failure surface tends to propagate along the direction of maximum shear stress, which is approximately linear, the angle with the horizontal plane is denoted as θ, the tunnel radius is denoted as r, h

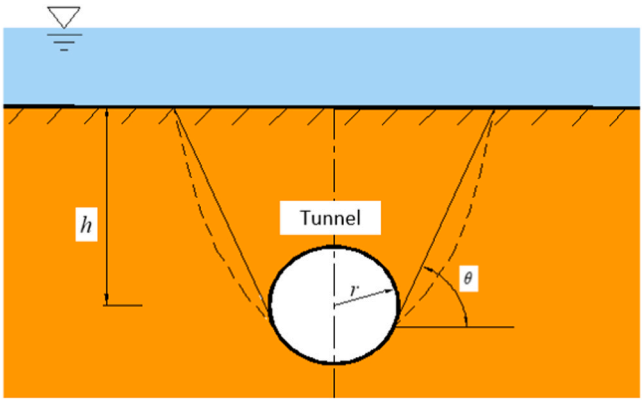

Fig. 1. Calculation model of formation collapse water inrush.

represents the thickness of the overlying layer. The stress components at any point on the slip surface can be expressed as:

$$\begin{cases} \sigma_n = \dfrac{\sigma_x+\sigma_y}{2} + \dfrac{\sigma_x-\sigma_y}{2}\cos 2\theta' - \tau_{xy}\sin 2\theta' \\ \tau_n = \dfrac{\sigma_x-\sigma_y}{2}\sin 2\theta' + \tau_{xy}\cos 2\theta' \quad \# \\ \theta' = 90^\circ - \theta \end{cases} \tag{1}$$

In the equation, σ_x, σ_y, and τ_{xy} represent the stress components in the surrounding rock induced by tunnel excavation.

By integrating Eq. (1) along the solid line, the shear force T_n on the slip surface is obtained. The shear strength at any point on the slip surface is calculated according to the Mohr-Coulomb criterion, yielding the critical shear force T_f on the slip surface:

$$T_n = \int_L \tau_n dL\# \tag{2}$$

$$T_f = \int_L (\mu\sigma_n + c)dL\# \tag{3}$$

Where L is the integration path along the solid line, μ is the friction coefficient, and c is the cohesion. Using the above physical quantities, the safety factor function of the slip surface can be defined as:

$$F = T_f - T_n\# \tag{4}$$

At this point, the potential strata slip surface angle θ_0 can be determined by setting the derivative of the safety factor function F with respect to the slip angle θ equal to zero.

The following section focuses on the overlying strata of the tunnel as the research subject, and derives the critical thickness of the tunnel's overlying strata in underwater tunnels based on catastrophe theory. The forces acting on the strata are calculated using the original rock stress. At this point, the gravitational force G, frictional force f, and seepage force F acting on the overlying strata can be expressed as:

$$G = \left(\frac{h^2 l}{\tan\theta_0} + 2rhl - \pi r^2 l\right)\gamma\# \tag{5}$$

$$f = 2\int_0^h l[K_0\gamma z\cos\theta + (\mu K_0\gamma z + c)\sin\theta]\frac{dz}{\sin\theta_0}\# \tag{6}$$

$$F = \left(\frac{h}{\tan\theta_0} + 2r\right)hlJ\gamma_w\# \tag{7}$$

In the equation, h represents the thickness of the overlying layer, r is the tunnel radius, l is the length of the unsupported section of the tunnel, γ is the unit weight of the rock mass, γ_w is the unit weight of water, K_0 is the lateral pressure coefficient, and J is the hydraulic gradient, z represents the elevation of the hydraulic head. Based on the ultimate equilibrium conditions of the strata, the following equation can be derived:

$$f = G + F\# \tag{8}$$

Substituting Eqs. (5) to (7) into the above expression, we obtain:

$$a_2h^2 + a_1h + a_0 = 0\# \tag{9}$$

Where:

$$a_0 = -\pi r^2 l\gamma\# \tag{10}$$

$$a_1 = 2rl(J\gamma_w + \gamma) - 2cl\# \tag{11}$$

$$a_2 = \frac{(\gamma + J\gamma_w - 2K_0\gamma)}{\tan\theta_0}l - 2\mu K_0\gamma l\# \tag{12}$$

Substituting $x = h + a_1/2a_2$ into Eq. (9) and simplifying, the surface equation for the folding-type catastrophe can be obtained as:

$$3x^2 + \alpha = 0\# \tag{13}$$

Where:

$$\alpha = 3\left(\frac{a_0}{a_2} - \frac{a_1^2}{4a_2^2}\right)\# \tag{14}$$

At this point, the potential function corresponding to Eq. (13) is:

$$V(x) = x^3 + \beta x\# \tag{15}$$

According to catastrophe theory, the critical point of stratum collapse in underwater tunnels occurs at $\alpha = 0$ and $x = 0$, where:

$$x = h + \frac{a_1}{2a_2} = 0 \tag{16}$$

Substituting Eqs. (11) and (12) into the above expression, the critical thickness of the overlying strata is obtained as:

$$h_{cr} = -\frac{a_1}{2a_2} = \frac{[r(J\gamma_w + \gamma) - c]\tan\theta_0}{2K_0\gamma(1 + \mu\tan\theta) - \gamma - J\gamma_w} \tag{17}$$

2.2.2. *The evolution mechanism of stratum collapse-type water inrush*

Research has shown that after yielding of the geotechnical materials, they typically exhibit strain-softening characteristics. The associated mechanical parameters undergo significant changes as plastic strain increases, primarily reflected in the elastic modulus E, cohesion c, and internal friction angle ϕ. These parameters are defined as functions of the equivalent plastic strain, where the equivalent plastic strain can be expressed as:

$$de^{ps} = \sqrt{\frac{(de_1{}^{ps} - de_m{}^{ps})^2 + (de_m{}^{ps})^2 + (de_3{}^{ps} - de_m{}^{ps})^2}{2}} \tag{18}$$

According to the Kozeny-Carman equation, the relationship between the permeability of a saturated porous medium and volumetric strain can be expressed as:

$$k = k_0\frac{1}{1+\varepsilon_v}\left(1 + \frac{\varepsilon_v}{n_0}\right)^3 \tag{19}$$

In the equation, ε_v represents the volumetric strain; k_0 denotes the initial permeability; and n_0 is the initial porosity.

Based on the above formula, a stress-permeability coupling analysis is conducted using FEM, with the Mohr-Coulomb criterion applied. The study focuses on a tunnel with a radius of 7.5 m, and an overlying water layer with a depth of 30 m. The initial parameters of the surrounding rock include an elastic modulus $E_0 = 1.4$ GPa, Poisson's ratio $\mu = 0.3$, internal friction angle $\phi_0 = 30$, cohesion $c_0 = 0.3$ MPa, dilatancy angle $\psi = 18°$, porosity of 0.2, and permeability of 1.0×10^{-6} cm/s. The

normal displacements at the left, right, and bottom boundaries of the model are fixed, with a surface water head of 30 m and a tunnel boundary water head of 0. The mechanical parameter degradation of the surrounding rock during the failure process is considered, and the surrounding rock enters the residual stage when the equivalent plastic shear strain reaches 1.0×10^{-4}.

The calculation results show that the evolution process of the stratum collapse-type water inrush in an underwater tunnel is illustrated in Fig. 2, and can be divided into four stages: In the first stage, shear failure occurs in the surrounding rock under concentrated stress. In the second stage, the shear strain range expands, with shear failure occurring on both sides, and hydraulic fracturing is triggered under water pressure. In the third stage, when the overlying soil layer thickness is less than the critical roof thickness, the shear strain at the crown increases and develops upwards, connecting with the hydraulic fracture at the ground surface. In the fourth stage, a water inrush channel is formed, and the shear slip zones on both sides of the tunnel connect with the ground surface, resulting in stratum collapse and triggering a water inrush disaster.

As shown in Fig. 3, the evolution of the tunnel crown and ground surface settlement over time exhibits a clear consistency: From 0–8 seconds, both the ground surface and tunnel crown settlements increase slowly with time; from 8 to 10 seconds, prior to the formation of the shear bands, the deformation rate begins to increase; after 10 seconds, during the formation of the shear bands, the deformation rate rapidly increases, ultimately leading to the collapse of the surrounding rock.

3. Numerical simulation analysis of surge water accidents

In order to determine the cause of the stratum collapse, this section will focus on the stability of the strata, surrounding rock reinforcement measures, and construction methods. The FEM model is employed to perform numerical simulations on the collapsed segment of the tunnel. Models will be established with optimized strata parameters, grouting rings, and improved construction methods. We analyse the plastic zone distribution, initial support stress, and crown settlement in the right-line tunnel by comparing the original and modified models , the feasibility of the prediction model is evaluated. The fundamental causes and mechanisms of surrounding rock instability in the Shijingshan Tunnel will be explored.

3.1. Project overview

The tunnel of Section 1 of the southern segment of the Xingye Expressway passes beneath the Shijingshan of the Jida Reservoir. The strata, from top to bottom, primarily consist of: artificial fill, alluvial deposits, colluvial layers, residual soils, completely weathered granite, strongly weathered granite, moderately weathered granite, and fractured granite, as shown in Fig. 4.

During the tunnel excavation process, the strength of the strata decreased, with the thickness of the strongly weathered and completely weathered limestone layers increasing. A weathered deep trough, reaching a maximum depth of 72.45 m, also developed. Within this weathered trough, the surrounding rock was weak, with a large-scale fragmented rock mass, a high degree of fissure development, and poor surrounding rock stability. According to the previous research, collapse-type water inrush is characterized by two factors. First, the tunnel traverses weak, fractured rock masses. Second, the overlying rock layer is thinner than the critical thickness. The water inrush zone of the right-line tunnel collapses from the weathered trough toward the excavation rear. The collapse zone intersects with the weathered trough and primarily traverses strongly weathered granite, with numerous fractures. The overlying artificial fill contains groundwater, which is stored in the pore spaces of loose soil and fractures in the weathered granite, forming multiple permeable channels. Due to the disturbance caused by excavation, the surrounding rock fissures develop and interconnect, forming drainage channels. This results in a hydraulic connection between surface water and the bedrock fracture water, and the thickness of the overlying rock and soil layers in the collapse zone is small, resulting in high water pressure. Therefore, it is concluded that the water inrush incident in the Shijingshan Tunnel is a collapse-type water inrush.

3.2. Basic conditions of numerical simulation

The distribution of each stratum is shown in Fig. 5. Advanced geological drilling in the interval strata measured a 24-hour stable groundwater table depth with an average value of 2.84 m and an average elevation of 30.41 m. According to regional empirical data, the annual variation range of the groundwater level in the survey area is 2.5 m. The parameters for each rock layer were determined based on supplementary investigation data, as shown in Table 1.

To account for the weakening effect of seepage on the mechanical

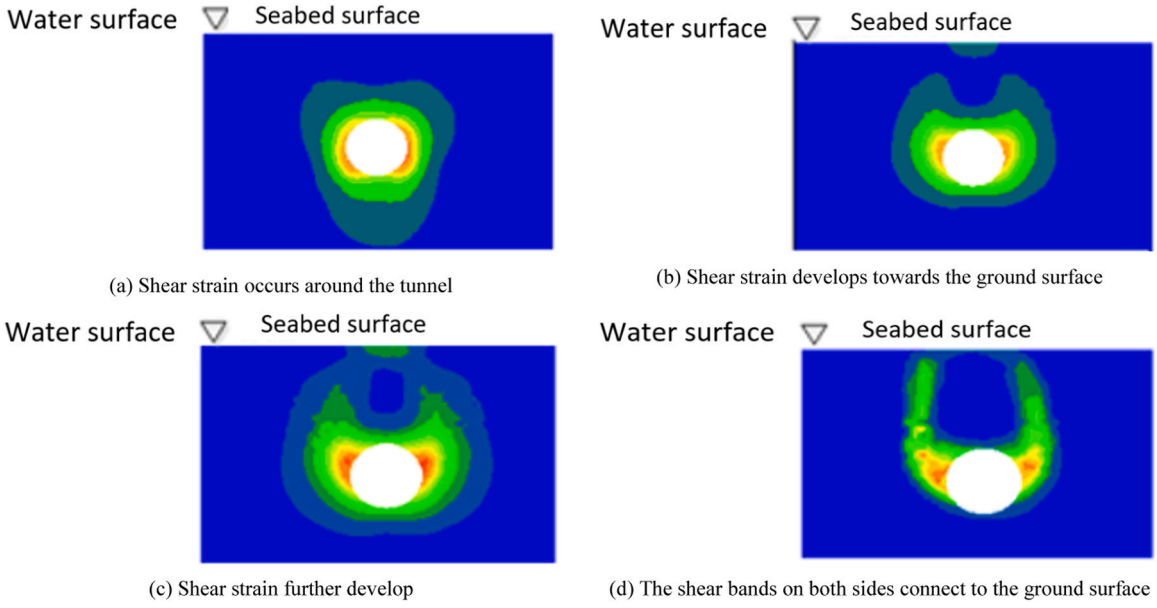

(a) Shear strain occurs around the tunnel

(b) Shear strain develops towards the ground surface

(c) Shear strain further develop

(d) The shear bands on both sides connect to the ground surface

Fig. 2. Evolution process of formation collapse water inrush via FEM.

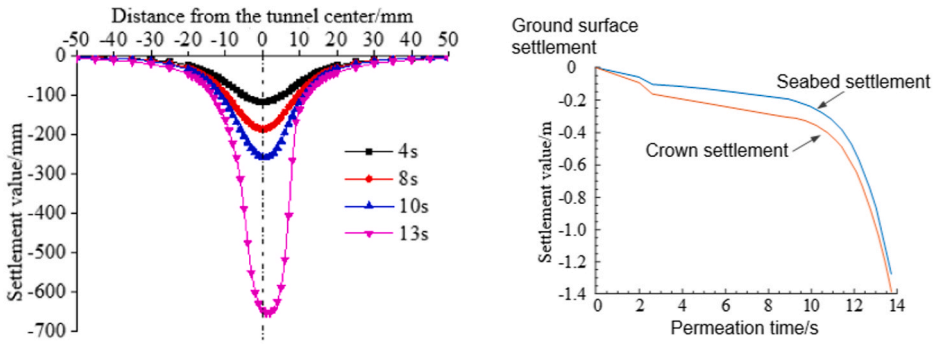

(a) Ground surface settlement variation. (b) Correspondence between ground surface and crown settlement.

Fig. 3. Evolution characteristics of ground deformation during formation collapse water inrush.

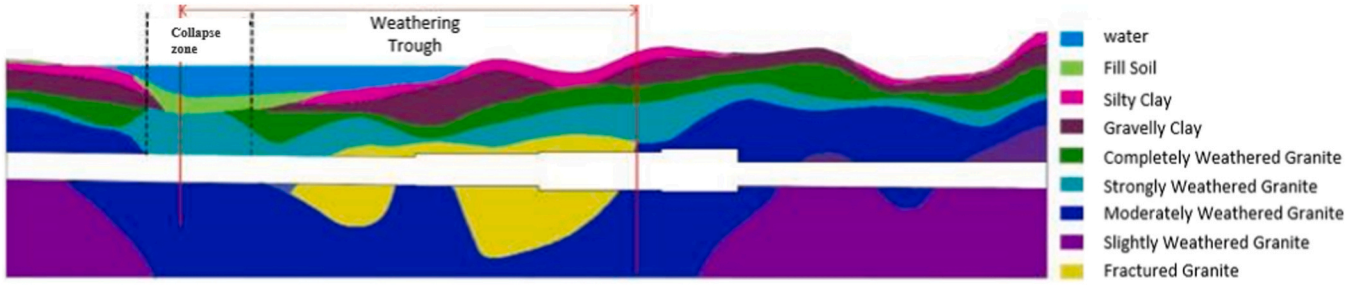

Fig. 4. Longitudinal section diagram of the right tunnel line.

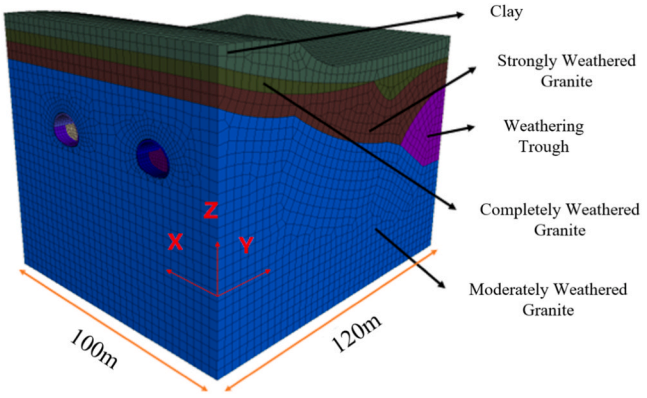

Fig. 5. Geological cross-section diagram.

properties of the surrounding rock, this study employs an effective stress-damage coupling model to dynamically reduce rock parameters [44]. The specific steps are as follows:

Based on Terzaghi's effective stress principle, pore water pressure u_w reduces the effective stress of the surrounding rock, expressed as:

$$\sigma' = \sigma - u\mathrm{w}\cdot I \tag{20}$$

This leads to the degradation of shear strength parameters (cohesion c and internal friction angle ϕ) in the Mohr-Coulomb criterion.

A damage factor $D \in [0,1]$ is defined to characterize fracture propagation induced by seepage. It is related to equivalent plastic strain de^{ps} and porosity change Δn:

$$D = 1 - \exp(-\alpha\cdot de^{ps} - \beta\cdot\Delta n) \tag{21}$$

where calibration parameters $\alpha = 2.5$ and $\beta = 0.8$ are determined through triaxial seepage tests.

Dynamic Reduction of Parameters:

$$\mathrm{c}' = \mathrm{c}_0\cdot(1 - D) \tag{22}$$

$$\tan\varnothing' = \tan\varnothing_0\cdot(1\text{-}0.6D) \tag{23}$$

$$E' = E_0\cdot(1\text{-}0.3D) \tag{24}$$

As shown in Fig. 6, the scale of the calculation model is 120 m × 100 m, with a depth of 50 m from the tunnel bottom to the model bottom and 17–27 m from the crown to the ground surface, totalling 197,000 elements. The construction adopts the bench excavation method, with each bench measuring 4 m in length and progressing 1 m per calculation step. The initial support is delayed by one step behind the face and is applied layer by layer, while the secondary lining is delayed by 8 steps behind the face and completed in a single step. Based on the

Table 1
Model parameters.

Structural Name	Model	Elastic Modulus /GPa	Poisson's Ratio	Cohesion /kPa	Friction Angle /(°)	Dilatancy Angle /(°)	Permeability Coefficient /(cm·s^{-1})
Fractured Granite	Mohr-Coulomb	0.3	0.36	50	20	10	1.0×10^{-4}
Completely Weathered Granite	Mohr-Coulomb	0.5	0.35	100	22.4	5	1.0×10^{-3}
Strongly Weathered Granite	Mohr-Coulomb	1	0.3	150	29	8	1.0×10^{-4}
Moderately Weathered Granite	Mohr-Coulomb	5	0.26	1000	38	15	1.0×10^{-5}
Soil Layer	Mohr-Coulomb	0.08	0.4	20	12	5	1.0×10^{-8}
Lining	Elasticity	30	0.2	—	—	—	—

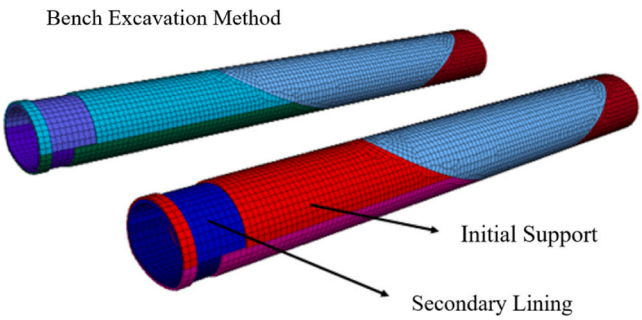

Fig. 6. Bench excavation method diagram.

theoretical analysis in the previous section, the mechanism of collapse-type water inrush in the strata is mainly caused by the sliding of the shear zone, resulting in stratum collapse. An elastic-plastic model (Mohr-Coulomb) is adopted for the constitutive relationship of the surrounding rock [45]. The interaction between the seepage field and stress field is also considered, with parameters shown in Table 1. The overburden thickness h in the numerical simulation corresponds to the critical thickness h_{cr} in the theoretical model. The hydraulic gradient J and permeability coefficient k in the theoretical model are dynamically coupled through the initial water head and tunnel boundary water head set in the simulation. The equivalent plastic strain de^{ps} in the theoretical model is intuitively validated by analyzing the plastic zone expansion path in the simulation. To explore the cause of stratum collapse, the impacts of strata stability, surrounding rock reinforcement measures, and construction methods on strata failure are examined. Regarding strata stability, the strata parameters are optimized to Grade III surrounding rock parameters, the properties of the weathered trough surrounding rock are modified to moderately weathered granite. Regarding surrounding rock reinforcement measures, a 3 m thick advance grouting reinforcement layer is added outside the initial support, with the grouting ring preceding the face by 4 m. Regarding the construction method, the bench excavation method is replaced with the sectional excavation method.

3.3. Numerical simulation results and analysis

3.3.1. Plastic zone of the surrounding rock

As shown in Figs. 7 and 8, the distribution of the plastic zone around the tunnel mainly involves two aspects: first, the boundary between the water-bearing soil layer under water pressure and the surrounding rock of different properties [46]; and second, certain regions of the surrounding rock near the tunnel face. The plastic zone is primarily characterized by tensile failure, with only a few localized shear failures occurring at the crown and near the tunnel face. Shear and tensile failures simultaneously occur at the contact surfaces between the surface, strongly weathered granite, and moderately weathered granite, as well as at the tunnel face. Among them, the plastic zones at the boundary between the surface and different surrounding rocks have little impact on surrounding rock instability [47]. According to Eq. (17), the numerically simulated ultimate roof thickness is calculated to be 21.5 m.

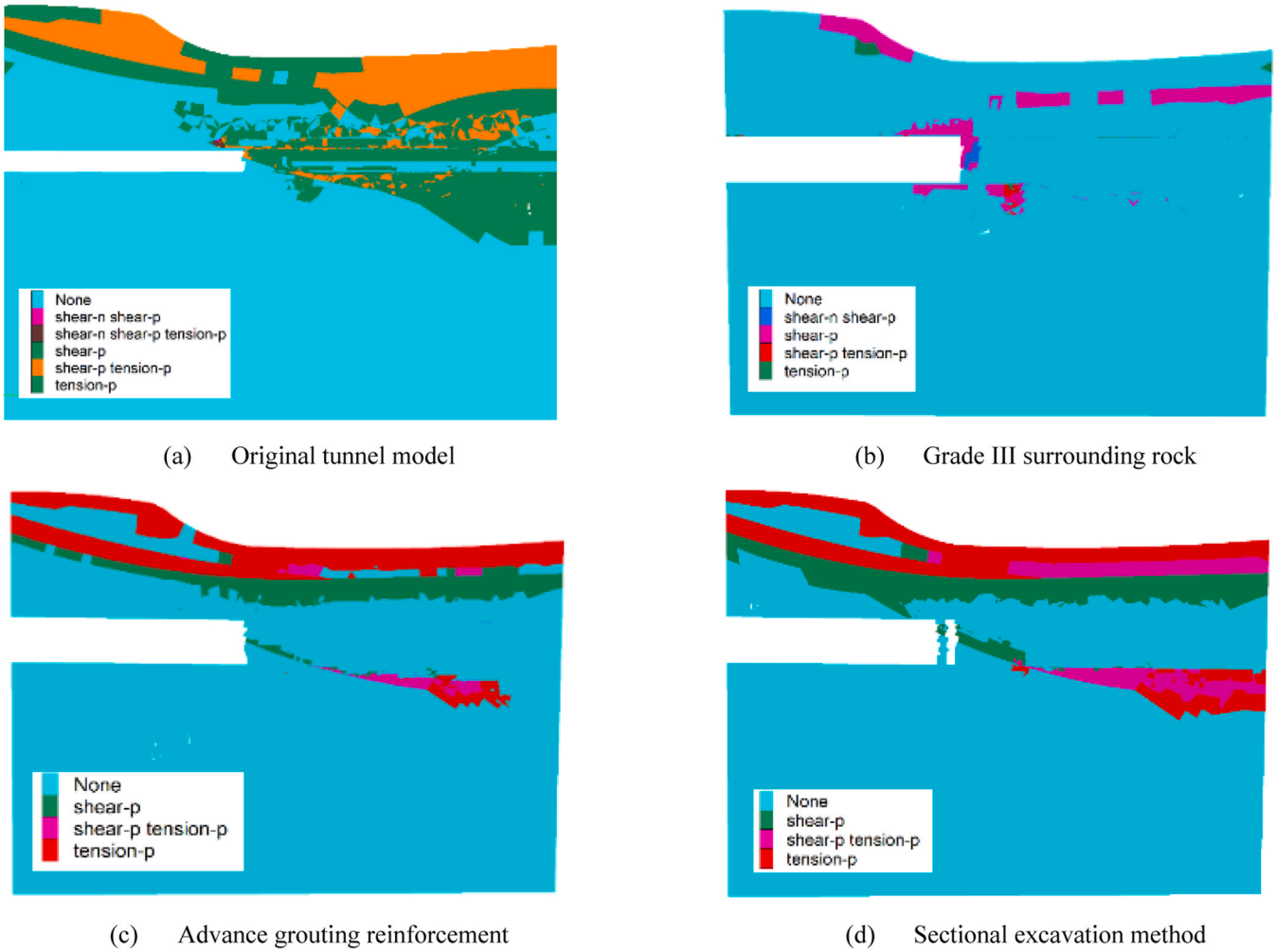

Fig. 7. Plastic zone in the right tunnel line.

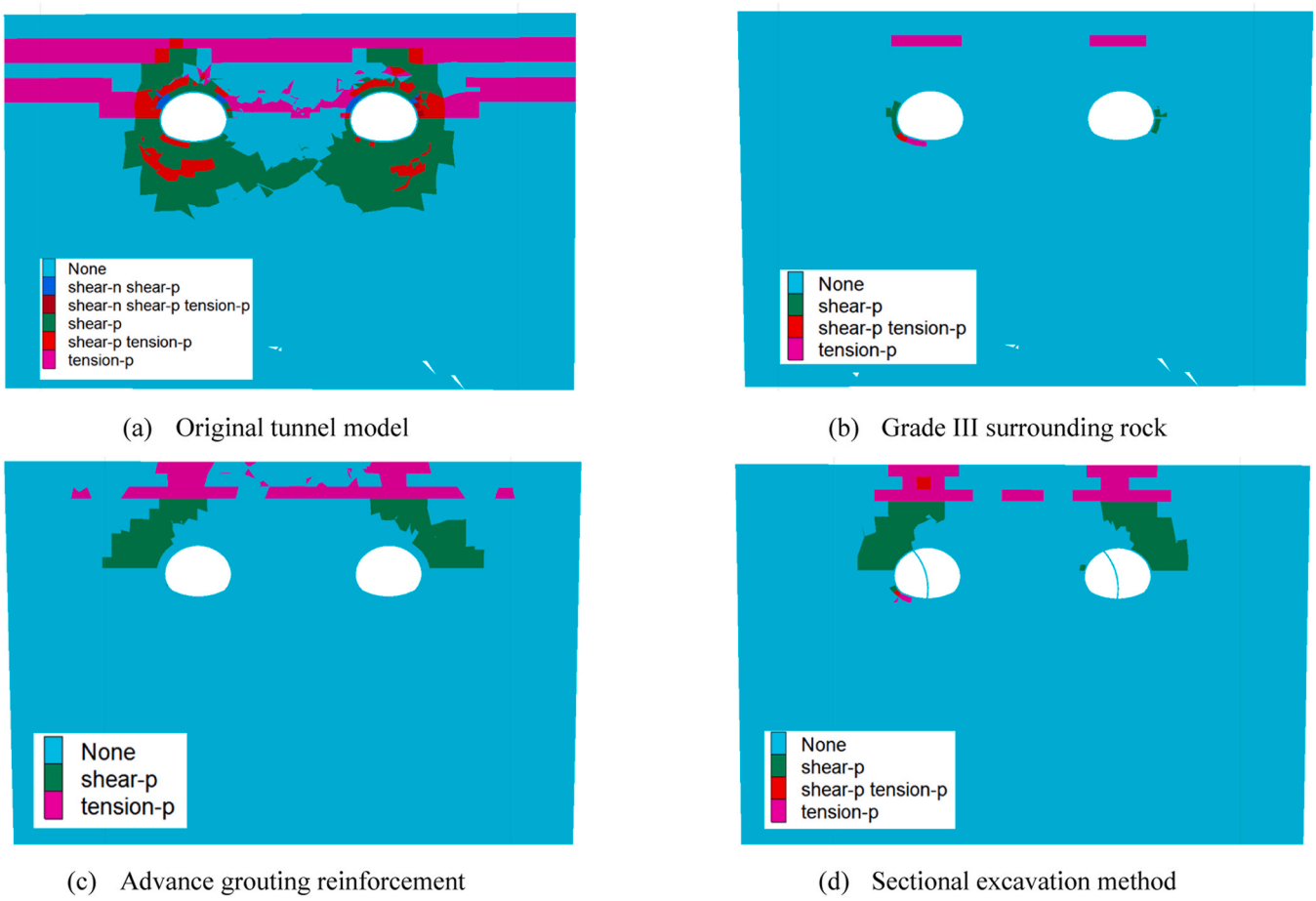

Fig. 8. Plastic zone in the tunnel cross-section.

In the numerical model, the overburden thickness ranges from $h = 17 - 27$ m. When $h < h_{cr}$, the numerical simulation results indicate that a water inrush channel forms. Conversely, when $h > h_{cr}$, the plastic zone does not extend to the surface. This consistency confirms the reasonableness of the parameter mapping and validates the reliability of the model through cross-verification. In the original condition (Figs. 7(a) and 8(a)), many plastic zones in front of the tunnel face are connected to the surface, forming sliding surfaces of collapse, leading to high susceptibility to surrounding rock instability. After improving the surrounding rock stability (Figs. 7(b) and 8(b)), the plastic zone in the Grade III surrounding rock condition is significantly reduced. Confined to the surface and the boundary between different surrounding rocks, indicating that enhancing stability can prevent surrounding rock failure. With the application of advance grouting reinforcement (Figs. 7(c) and 8(c)), the range of the plastic zone is significantly reduced and remains unconnected, thus preventing surrounding rock failure. However, since the advance grouting only acts within a certain range in front of the tunnel face, there still exists a large plastic zone in areas not reinforced by grouting. After switching to sectional excavation (Figs. 7(d) and 8(d)), the plastic zone is significantly reduced, and the plastic connected zones around the tunnel are located behind the tunnel face. At this point, the initial support has been applied, increasing the support strength, and the surrounding rock will not collapse. In addition to improving surrounding rock stability, advance grouting reinforcement can reduce the connection between surface water and the tunnel plastic zone caused by fractures. This enhances surrounding rock stability within a certain range. Compared to the sectional excavation method, enhancing the support strength is more effective in controlling surrounding rock instability.

3.3.2. *Initial support stress*

According to experience, the tensile strength of concrete is typically 5–10 % of its compressive strength. Considering the effect of hardening time, the tensile strength is set to 1 MPa. The blue area in the figure represents tensile stress less than 1 MPa, where no failure has occurred; the coloured areas represent tensile stress greater than 1 MPa, where failure has occurred. A cross-section located 5 m from the tunnel face, where the initial support has just been completed, is selected for analysis.

As shown in Fig. 9(a), the maximum tensile stress reaches 6.94 MPa. Both the upper and lower edges of the left arch shoulder exceed the tensile strength and are connected, indicating failure of the initial support. By organizing Figs. 9 and 10, the maximum tensile and compressive stresses for each condition are obtained and listed in Table 2. After improving the surrounding rock stability, the maximum tensile stress in the tunnel cross-section is reduced from 6.94 MPa to 0.65 MPa, which is less than 1 MPa, and no tensile failure occurs. The maximum compressive stress decreases from 11.78 MPa to 2.69 MPa. The maximum tensile stresses of the initial support for advance grouting reinforcement and sectional excavation are 1.14 MPa and 1.71 MPa, respectively. Although these exceed 1 MPa, they do not surpass 5 % of the ultimate compressive strength, and the failure zones are not connected (Fig. 9(c) and (d)), so no tensile failure occurs. Since the maximum compressive stress in all three modified conditions is much lower than the ultimate compressive strength of C30 concrete, the initial support does not fail. The control effect ranks as: Grade III surrounding rock > advanced grouting > sectional excavation. Due to the change in the strata properties and the variation in the reservoir water depth, the load on the tunnel has significantly increased, but the design strength of the initial tunnel support remains unchanged, leading to failure.

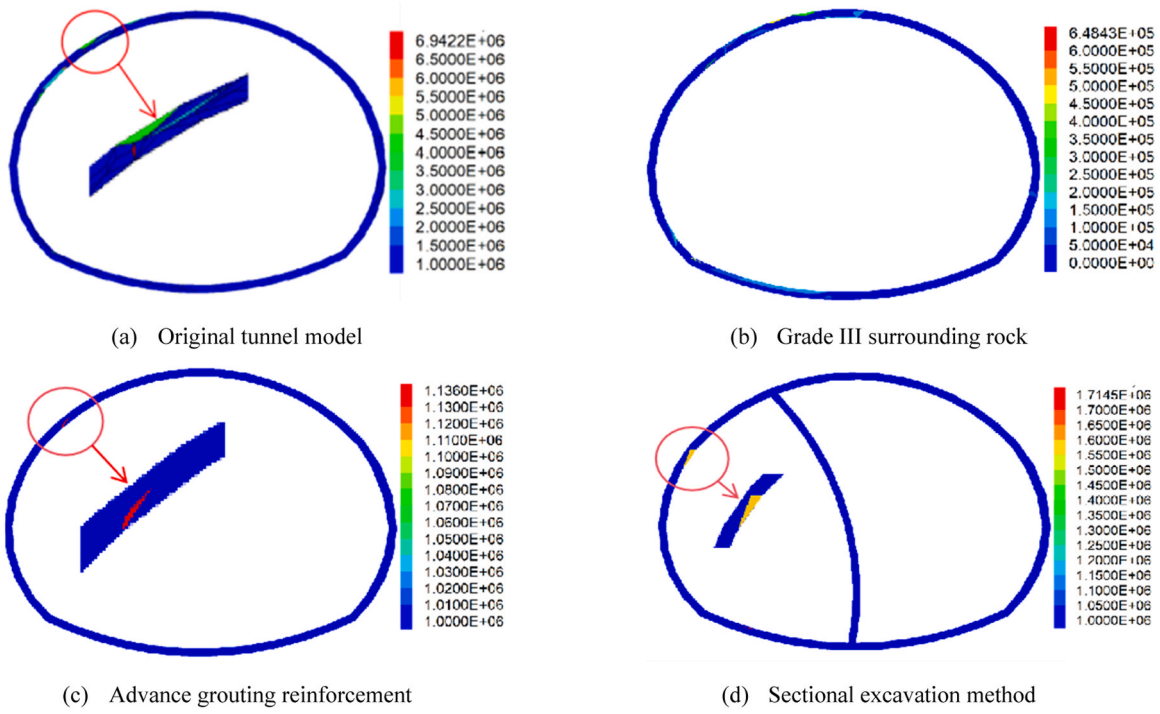

Fig. 9. Major principal stress in the right tunnel line cross-section.

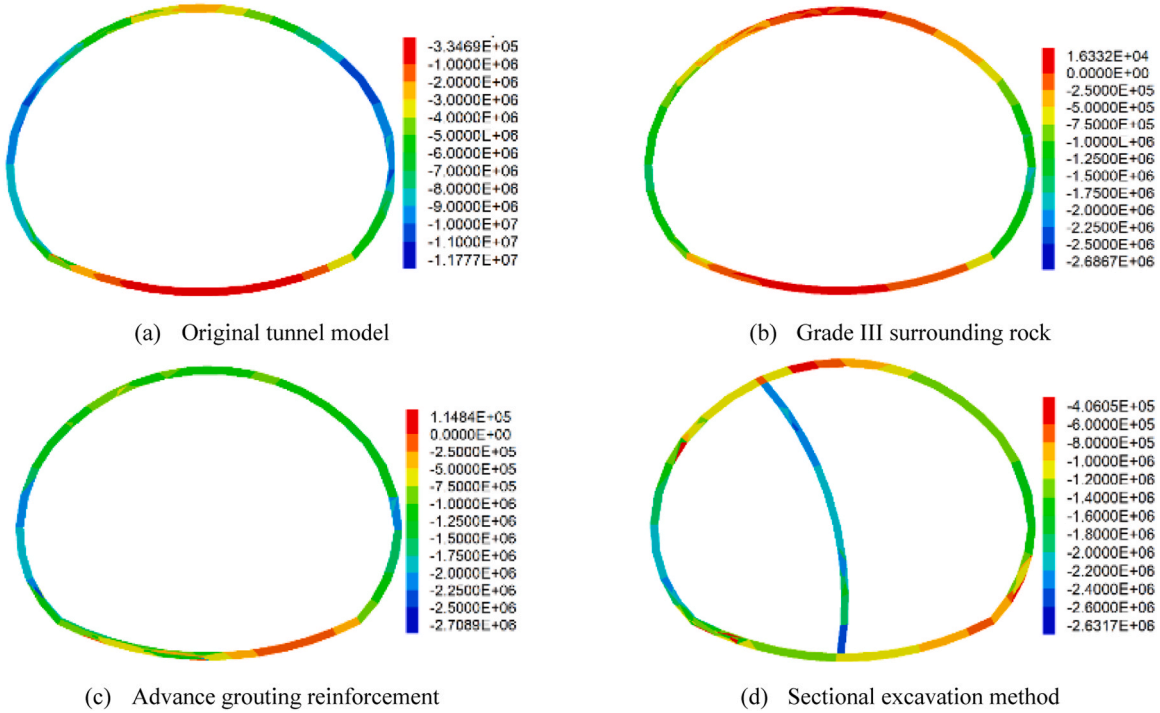

Fig. 10. Minor principal stress in the right tunnel line cross-section.

3.3.3. Vertical deformation of the surrounding rock

As shown in Fig. 11, the vertical deformation of the surrounding rock is primarily seen as crown settlement and floor heave. Crown settlement is more pronounced, indicating significant disturbance to the crown during tunnel excavation. Notably, under the original condition, the maximum settlement of the tunnel crown occurs near the tunnel face, rather than in the area where the initial support has been completed. This suggests poor surrounding rock conditions and the occurrence of advance failure, as the original support scheme failed to provide sufficient support to resist the deformation of the surrounding rock. Table 3 presents the maximum deformation for each working condition, along with the extent of reduction relative to the original condition. The maximum deformation at the tunnel crown is reduced from 5.52 cm to 0.48 cm, achieving a 90 % reduction. After improving surrounding rock stability through advance grouting reinforcement or sectional excavation, the maximum crown deformation is significantly smaller than in

Table 2
Maximum stress in the tunnel cross-section.

Working Condition	Maximum Tensile Stress/MPa	Maximum Compressive Stress/MPa
Original tunnel model	6.94	11.78
Grade III surrounding rock	0.65	2.69
Advance grouting reinforcement	1.14	2.71
Sectional excavation method	1.71	2.63

the original condition. The reduction magnitude is ranked as: Grade III surrounding rock > sectional excavation > advance grouting reinforcement. In addition to improving surrounding rock stability, replacing bench excavation with sectional excavation reduces construction disturbance during tunnel excavation [48]. Compared to advance grouting, sectional excavation provides better control over surrounding rock deformation by preventing advance failure.

4. Accident analysis

4.1. Risk assessment

The Shijingshan Tunnel is located in a complex geological area, with surrounding rocks in Grade III to V, and the tunnel crosses a weathered zone. The rock and soil mass within the zone consists of fractured granite, which has high permeability, thereby increasing the risk of water inrush. (Fig. 12, Fig. 13)

Based on the risk grade determined by the permeability coefficient (Table 4) and actual monitoring data, the permeability coefficient of the geological body in the tunnel section is 1.5×10^{-4} cm/s [15,49]. This indicates moderate permeability and a relatively high safety risk. This also suggests the potential for localized water inrush or collapse. The permeability coefficient of the Shijingshan Tunnel places it in a high-risk zone, particularly in the weathered zone where the rock mass has fissures. Water pressure is transmitted through the fissure network, increasing the risk of surrounding rock failure.

Numerical simulations show that as excavation progresses, the surrounding rock of the right-line tunnel gradually enters the plastic failure

Table 3
Maximum deformation of the tunnel crown.

Working Condition	Maximum Deformation /cm	Reduction Magnitude /(%)
Original tunnel model	5.52	—
Grade III surrounding rock	0.48	90
Advance grouting reinforcement	1.82	67
Sectional excavation method	1.51	73

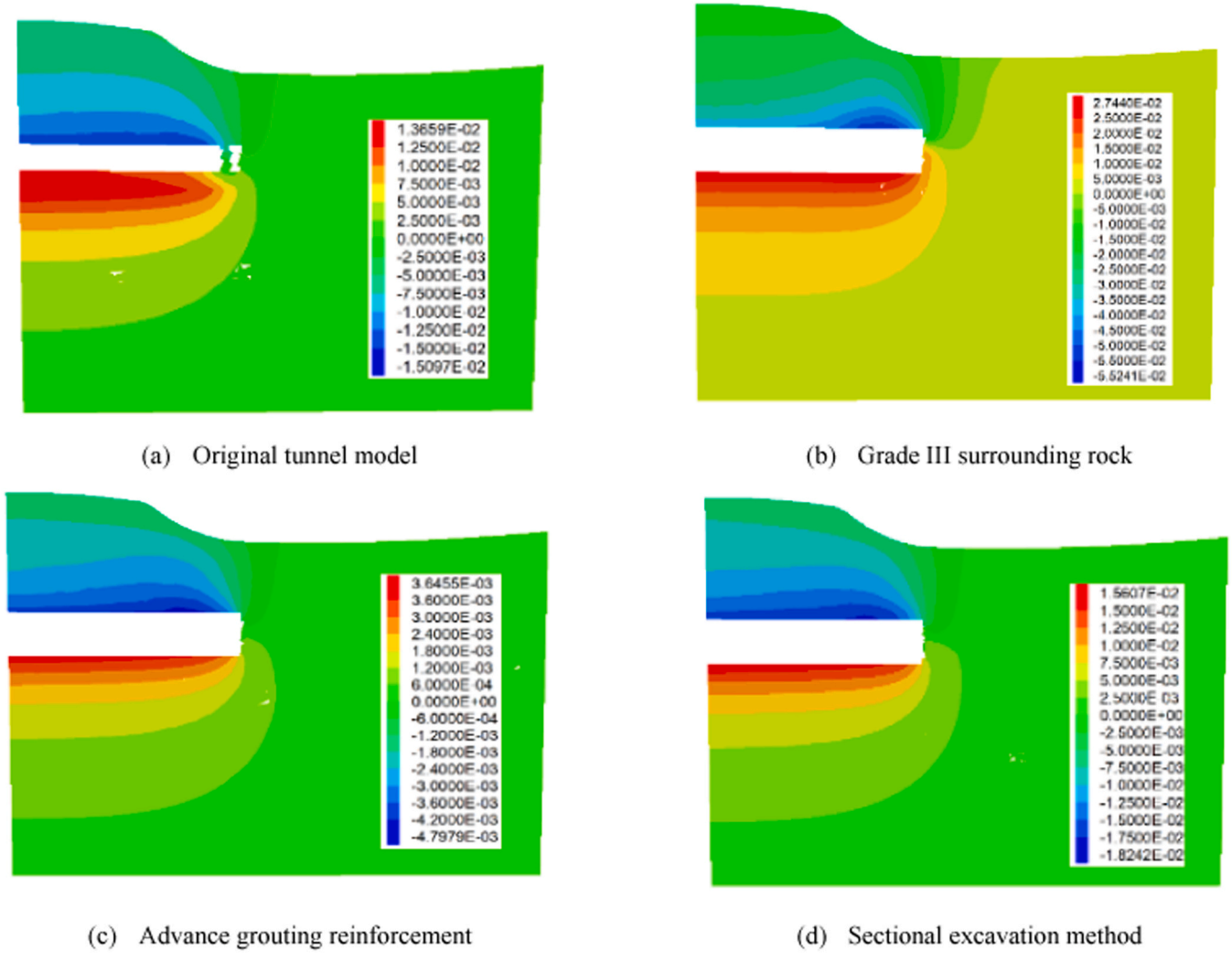

Fig. 11. Longitudinal distribution of settlement in the right tunnel line.

(a) Upper bench excavation face of the right pilot tunnel (b) Upper bench excavation face of the left pilot tunnel

Fig. 12. The schematic diagram of seepage trace on tunnel face.

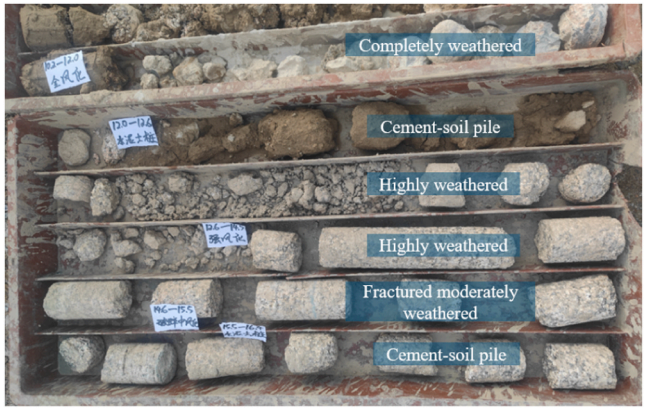

Fig. 13. Core samples of rock from borehole.

Table 4
Water inrush risk classification of tunnels.

Risk Grade	Permeability coefficient /(m·s^{-1})	Permeability description	Disaster scale description
I	$> 1 \times 10^{-4}$	High permeability	A large-scale water inrush or collapse may occur.
II	1×10^{-7}~1×10^{-4}	Moderate permeability	Localized water inrush or collapse may occur.
III	1×10^{-8}~1×10^{-7}	Low permeability	Fracture-induced water inrush may occur.
IV	$< 1 \times 10^{-8}$	Very low permeability	No significant risk of water inrush.

zone. This is particularly evident between the RK2 + 005 and RK2 + 035 sections, where surrounding rock strength decreases and the plastic zone expands. The development of the fracture network causes water pressure to directly act on the tunnel support structure, increasing its risk of failure. In such an environment with high water pressure and weak surrounding rock, the existing initial support cannot effectively resist the surrounding rock settlement and heave, leading to an increased risk of water inrush and collapse. To mitigate the risk, it is recommended to enhance advance grouting in high-risk areas and reinforce the initial support structure.

4.2. Causes of water inrush

When crossing the weathered zone, the stratum in which the tunnel is located consists of fully weathered granite and fractured granite, with developed fissures. Groundwater flows along these fissures, forming multiple permeable channels. Borehole survey results indicate that the groundwater level in the reservoir area is relatively high, and some fissures are connected to the weathered zone of the tunnel surrounding rock. Groundwater flows into the tunnel through these fissures, leading to the occurrence of the water inrush incident.

Numerical simulations confirm that when the right-line tunnel approaches the weathered zone, as shown in Fig. 14, the rock strength significantly decreases, fissures expand, and the tensile stress on the tunnel crown and sidewalls exceeds the support design limits. The surrounding rock is unable to resist water pressure, ultimately leading to collapse and water inrush. Particularly in the RK2 + 010 section, the settlement of the tunnel crown and heave of the base slab are particularly pronounced. Combined with the weakened bearing capacity of the strata and the sharp increase in groundwater pressure, water inrush becomes an inevitable consequence. Based on numerical simulations and field conditions, the main cause of the water inrush in the tunnel is the complex geological conditions and the sudden increase in groundwater pressure. To prevent similar incidents in future construction, it is recommended to implement advance reinforcement in weathered zones and high water pressure areas. Additionally, optimizing the initial

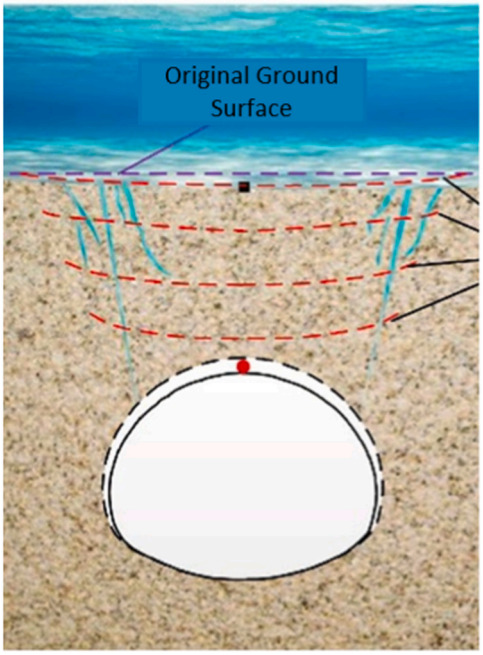

Fig. 14. Longitudinal distribution of settlement in the right tunnel line.

support design and applying advance grouting will reduce the risk of water inrush.

5. Conclusion

To investigate the cause of the water inrush accident in the Shijingshan Tunnel, a stratum collapse-induced water inrush analysis and prediction model based on catastrophe theory was proposed. Numerical models under different working conditions are established using the FEM. The feasibility of the prediction model is evaluated by comparing the development of plastic zones in the surrounding rock, deformation patterns, and support stress responses. Numerical results indicate that, after tunnel excavation, the surrounding rock undergoes shear failure under concentrated stress, while hydraulic fracturing occurs at the surface due to water pressure. When the thickness of the overlying strata is less than the critical roof thickness, upward-developing shear strains at the arch waist connect with surface fractures, forming a water inrush pathway. Meanwhile, shear slip zones on both sides of the tunnel link to the ground surface, leading to stratum collapse and triggering the water inrush hazard.

Based on the identified water inrush mechanism and site conditions, the Shijingshan Tunnel accident is determined to be a stratum collapse-induced water inrush. A fluid–solid coupling numerical model is established to analyse the cause of the incident. Four working conditions are designed from the perspectives of stratum stability, surrounding rock reinforcement, and construction methods: the original tunnel model, Grade III surrounding rock, advanced grouting reinforcement, and staged excavation. Numerical results indicate that the original condition presents a high risk, while the other three scenarios significantly reduce the extent of the plastic zone and vertical deformation, with intact support structures and no risk of collapse. Combined with the geological and construction conditions of the inrush section, the accident is attributed to low surrounding rock strength and surface water infiltration through connected fractures. Among the control measures, Grade III surrounding rock exhibited the best performance, followed by advanced grouting and staged excavation. This study provides a theoretical basis for assessing and mitigating water inrush risks during tunnel construction beneath water bodies.

CRediT authorship contribution statement

Chen Jiayao: Methodology. **Zhang Dingli:** Methodology. **Su Mingyue:** Validation. **Liu Xiaotian:** Writing – review & editing, Writing – original draft. **Mi Xiangdong:** Methodology.

Declaration of Competing Interest

The authors declare that they have no known competing financial interests or personal relationships that could have appeared to influence the work reported in this paper

Acknowledgments

The research presented in this paper is supported by Fundamental Research Funds for the Central Universities (No. 2023JBRC005), Natural Science Foundation Committee Program of China (Grant No. 52308388), opening fund of State Key Laboratory of Geohazard Prevention and Geoenvironment Protection (Chengdu University of Technology) (No. SKLGP2024K008), open project of State Key Laboratory of Performance Monitoring and Protecting of Rail Transit Infrastructure, East China Jiaotong University (No. HIGZ2023101).

References

[1] Z. Dingli, Essential issues and their research progress in tunnel and underground engineering, Chin. J. Theor. Appl. Mech. 49 (2017) 3–21.
[2] Ø. Dammyr, B. Nilsen, J. Gollegger, Feasibility of tunnel boring through weakness zones in deep Norwegian subsea tunnels, Tunn. Undergr. Space Technol. 69 (2017) 133–146.
[3] P. Perazzelli, T. Leone, G. Anagnostou, Tunnel face stability under seepage flow conditions, Tunn. Undergr. Space Technol. 43 (2014) 459–469.
[4] D.L. Zhang, Z.Y. Sun, H.R. Song, H.C. Fang, Water inrush evolutionary mechanisms of subsea tunnels and process control method, Chin. J. Rock. Mech. Eng. 39 (2020) 649–667.
[5] G. Fernandez, J. Moon, Excavation-induced hydraulic conductivity reduction around a tunnel–Part 1: Guideline for estimate of ground water inflow rate, Tunn. Undergr. Space Technol. 25 (5) (2010) 560–566.
[6] R.X. Shen, X.Y. Wu, C.W. Liu, D.J. Zeng, Research of water inrush on subsea tunnel construction, Chin. J. Wuhan. Univ. Technol. (Transp. Sci. Eng.) 32 (2008) 385–388.
[7] M. ZHANG, X. GAO, Y. GUO, Analysis of Water Inrush in Undersea Tunnel and Its Application in Xiang'an Tunnel, J. Beijing Univ. Technol. 33 (2007) 273–277.
[8] C. Cacciuttolo, A. Pastor, P. Valderrama, E. Atencio, Process water management and seepage control in tailings storage facilities: Engineered environmental solutions applied in Chile and Peru, Water 15 (1) (2023) 196.
[9] Z. Maleki, H. Farhadian, A. Nikvar-Hassani, Geological hazards in tunnelling: the example of Gelas water conveyance tunnel, Iran, Q. J. Eng. Geol. Hydrogeol. 54 (1) (2021) qjegh2019-114.
[10] F. Niu, Y. Cai, H. Liao, et al., Unfavorable geology and mitigation measures for water inrush hazard during subsea tunnel construction: A global review, Water 14 (2022) 1592.
[11] H. Farhadian, A. Nikvar-Hassani, Water flow into tunnels in discontinuous rock: a short critical review of the analytical solution of the art, Bull. Eng. Geol. Environ. 78 (2019) 3833–3849.
[12] A. Banerjee, S. Pasupuleti, M.K. Singh, S.C. Dutta, G.P. Kumar, Modelling of flow through porous media over the complete flow regime, Transp. Porous Media 129 (2019) 1–23.
[13] V. Vincenzi, A. Gargini, N. Goldscheider, Using tracer tests and hydrological observations to evaluate effects of tunnel drainage on groundwater and surface waters in the Northern Apennines (Italy), Hydrogeol. J. 17 (1) (2009) 135–150.
[14] J. Molinero, J. Samper, R. Juanes, Numerical modeling of the transient hydrogeological response produced by tunnel construction in fractured bedrocks, Eng. Geol. 64 (4) (2002) 369–386.
[15] J. Zhang, Y. Zhang, T. Liu, Rock Mass Permeability and Coal Mine Water Inrush, Geological Publ House Beijing, 1997, p. 36 (in Chinese).
[16] M. Florio, E. Sirtori, Social benefits and costs of large scale research infrastructures, Technol. Forecast. Soc. Change 112 (2016) 65–78.
[17] G.B. Grant, D. Drysdale, Estimating heat release rates from large-scale tunnel fires, *Fire Saf. Sci. -Proc. fifth Int. Symp.* . (1997, March) 1213–1224.
[18] F. Göktepe, I. Keskin, A comparison study between traditional and finite element methods for slope stability evaluations, J. Geol. Soc. India 91 (2018) 373–379.
[19] N. Fazio, M. Perrotti, G. Andriani, F. Mancini, P. Rossi, C. Castagnetti, P. Lollino, A new methodological approach to assess the stability of discontinuous rocky cliffs using in-situ surveys supported by UAV-based techniques and 3-D finite element model: a case study, Eng. Geol. 260 (2019) 105205.
[20] B. Brady, L. Lorig, Analysis of rock reinforcement using finite difference methods, Comput. Geotech. 5 (2) (1988) 123–149.
[21] Y.L. Zhao, P. Cao, Y.X. Wang, Y.K. Liu, Coupling model of seepage-damage-fracture in fractured rock masses and its application, Chin. J. Rock. Mech. Eng. 27 (2008) 1634–1643.
[22] S. Ghorbani, K. Bour, R. Javdan, M. Bour, Design of effective grouting pattern in Kerman water conveyance tunnel using DFN-DEM and analytical approaches, Int. J. Geosynth. Ground Eng. 9 (2) (2023) 19.
[23] D.U. Barboza, L.A. Bressani, Seepage Analysis of Concrete and Embankment Dam Abutment: A Case Study of the Ribeirão João Leite Dam, Geotech. Geol. Eng. (2024) 1–25.
[24] P.F. Li, D. Zhang, Y. Zhao, C. Zhang, Study of distribution law of water pressure acting on composite lining and reasonable parameters of grouting circle for subsea tunnel, Chin. J. Rock. Mech. Eng. 31 (2012) 280–288.
[25] M.R. Shekari, A coupled numerical approach to simulate the effect of earthquake frequency content on seismic behavior of submarine tunnel, Mar. Struct. 75 (2021) 102848.
[26] A. Fahimifar, M.R. Zareifard, A theoretical solution for analysis of tunnels below groundwater considering the hydraulic–mechanical coupling, Tunn. Undergr. Space Technol. 24 (6) (2009) 634–646.
[27] S. Haoran, Z. Dingli, F. Qian, Analytic solution on the stress of surrounding rocks for shallow subsea tunnel, China Civ. Eng. J. 48 (2015) 283–288.
[28] G. Tsinidis, F. de Silva, I. Anastasopoulos, E. Bilotta, A. Bobet, Y.M. Hashash, R. Fuentes, Seismic behaviour of tunnels: From experiments to analysis, Tunn. Undergr. Space Technol. 99 (2020) 103334.
[29] C.J. Booth, Groundwater as an environmental constraint of longwall coal mining, Environ. Geol. 49 (2006) 796–803.
[30] E. Colas, E.M. Klopries, D. Tian, M. Kroll, M. Selzner, C. Bruecker, F. Amann, Overview of converting abandoned coal mines to underground pumped storage systems: Focus on the underground reservoir, J. Energy Storage 73 (2023) 109153.
[31] S. Alija, F.J. Torrijo, M. Quinta-Ferreira, Geological engineering problems associated with tunnel construction in karst rock masses: The case of Gavarres tunnel (Spain), Eng. Geol. 157 (2013) 103–111.
[32] V.N. Odintsev, N.A. Miletenko, Water inrush in mines as a consequence of spontaneous hydrofracture, J. Min. Sci. 51 (2015) 423–434.

[33] S. Levasseur, R. Charlier, B. Frieg, F. Collin, Hydro-mechanical modelling of the excavation damaged zone around an underground excavation at Mont Terri Rock Laboratory, Int. J. Rock. Mech. Min. Sci. 47 (3) (2010) 414–425.
[34] J.N. Hutchinson, The Fourth Glossop Lecture: reading the ground: Morphology and geology in site appraisal, Q. J. Eng. Geol. Hydrogeol. 34 (1) (2001) 7–50.
[35] Martin, C.J., Morley, A.L., & Griffiths, J.S. (2017). Introduction to engineering geology and geomorphology of glaciated and periglaciated terrains.
[36] Z. Huang, Q. Zhong, Q. Gu, Y. Lin, K. Zhao, X. Zhang, Y. Wu, Numerical investigation of particle migration in fault zones during water and mud inrush using the CFD–DEM approach, Comput. Part. Mech. (2025) 1–17.
[37] H.H. Einstein, Risk and risk analysis in rock engineering, Tunn. Undergr. Space Technol. 11 (2) (1996) 141–155.
[38] S. Loew, G. Barla, M. Diederichs, Engineering geology of Alpine tunnels: Past, present and future, *Geol. Act. —Proc. 11th IAEG Congr.* (2010, September) 201–253.
[39] Q. Gu, Z. Huang, K. Zhao, W. Zhong, L. Liu, X. Li, M. Dan, Effects of high temperature and thermal cycles on fracture surface's roughness of granite: An insight on 3D morphology, J. Rock Mech. Geotech. Eng. 17 (2) (2025) 810–826.
[40] G.B. Hemphill, Practical Tunnel Construction, John Wiley & Sons, 2012.
[41] Priestley, S.C., Shand, P., Love, A.J., Crossey, L.J., Karlstrom, K.E., Keppel, M.N., … & Rousseau-Guetin, P. (2019). Hydrochemical variations of groundwater and spring discharge of the western Great Artesian Basin.
[42] Panthi, K.K. (2006). Analysis of engineering geological uncertainties related to tunnelling in Himalayan rock mass conditions.
[43] D.G. Price, A.B. Malkin, J.L. Knill, Foundations of multi-storey blocks on the Coal Measures with special reference to old mine workings, Q. J. Eng. Geol. Hydrogeol. 1 (4) (1969) 271–322.
[44] L.C. Li, C.A. Tang, G. Li, S.Y. Wang, Z.Z. Liang, Y.B. Zhang, Numerical simulation of 3D hydraulic fracturing based on an improved flow-stress-damage model and a parallel FEM technique, Rock. Mech. Rock. Eng. 45 (2012) 801–818.
[45] R.G. Mikola, K. Hatami, D. Doolin, Elastic–plastic discontinuous deformation analysis using Mohr–Coulomb model, Min. Technol. 120 (3) (2011) 148–157.
[46] G. Anagnostou, Tunnel stability and deformations in water-bearing ground. In *Proceedings of the international symposium of the international society for rock mechanics*, Taylor & Francis, *London*, 2006, April, pp. 3–13.
[47] M.S. Diederichs, P.K. Kaiser, E. Eberhardt, Damage initiation and propagation in hard rock during tunnelling and the influence of near-face stress rotation, Int. J. Rock. Mech. Min. Sci. 41 (5) (2004) 785–812.
[48] M. Sharifzadeh, F. Kolivand, M. Ghorbani, S. Yasrobi, Design of sequential excavation method for large span urban tunnels in soft ground–Niayesh tunnel, Tunn. Undergr. Space Technol. 35 (2013) 178–188.
[49] T. Li, Z. Wang, T. Peng, et al., The Professional Standards Compilation Group of People's Republic of China. Design specification for slope of hydropower and water conservancy project, 5353, China Electric Power Press, Beijing DL, 2006.

Dr. Jiayao Chen is Associate Professor in the School of Civil Engineering at Beijing Jiaotong University. He obtained his PhD degree in 2022 in Tongji University. His main research interests are risk assessment and control for tunnel engineering, construction risk pre-warning by AI-based Inspection, Long-term behaviour for tunnel and maintenance. He has been honoured as a Young Talent by the China Association for Science and Technology and is part of Beijing Jiaotong University's Young Talent Program. Dr. Chen has received recognition for his outstanding doctoral dissertation from the Chinese Society for Rock Mechanics and Engineering, as well as from Tongji University. He serves on the editorial boards of several prestigious journals, including the International Journal of Mining Science and Technology, the International Journal of Coal Science and Technology, and Deep Underground Science and Engineering, etc. He is also a board member and secretary of the Chinese Society of Civil Engineering Risk and Insurance Research Division, a member of the Youth Committee.